A TWO-DIMENSIONAL AERODYNAMIC MODEL FOR SUPER-HIGH-SPEED ELEVATOR DESIGN

H.W. Yang*, A.T.P. So**, T.T. Chow** and K.C. Lam**

* Beijing University of Aeronautics and Astronautics
** City University of Hong Kong

ABSTRACT

During Elevcon'96 held in Barcelona, a paper on the 1-dimensional aerodynamic model for super-high-speed elevator design was presented. That paper addressed the "weak shock" produced when the car was accelerating and that was the source of excessive vibration. In this paper, the unsteady 2-dimensional turbulence flow in the hoistway with an upward accelerating car is simulated by solving the time-dependent Navier-Stokes (N-S) equations with a corresponding turbulence model. Since the flow is very complicated due to unsteadiness, compressibility and strong turbulence, the numerical scheme must be highly efficient. Therefore, a new "multi-grid" method is adopted. The results of simulating three kinds of car shape, namely flat top, conical top and spherical top, show that this method has been very effective in solving such a complicated problem.

1 INTRODUCTION

As the cities are becoming more and more densely populated, buildings are getting higher and higher. The proposal of "kilometer-high building" was announced decades ago. Therefore, the demand for better services in vertical transportation within buildings is rapidly increasing because citizens live and work in higher and higher buildings. The highest building in the world is now slightly over 100 storeys but the concept of 'kilometer high' building has been under active consideration. In accordance with Fortune [2], the key to efficient, mega high-rise elevator design is to stack local zones served by their own local elevators on top of one another. These local zones are then served by very high-speed, sky-lobby shuttle elevators, serving express between the ground terminal floor(s) and the sky lobby(ies). With a view to this approach, the speed of elevators in the future will continuously be increasing. The rated speed record of 600 m/min was achieved in 1977 in Tokyo and then 750 m/min in 1993 in Yokohama. Now, elevators up to 840 m/min are being developed. It is not so difficult to increase the rated speed of drive motors or the gear ratio to achieve a higher rated speed for elevators. However, super-high-speed elevators suffer from two major mechanical problems, namely excessive vibration and aerodynamic noise.

The first problem is associated with the increasing drag force exerted by the high-speed air movement around an ascending or descending elevator car. These problems, which are generated from the aerodynamics of the system, hinder the development of higher speed elevators and they must be solved in order to make the vertical transportation keep

abreast with the construction of super-high-rise buildings in the next century. Human response is greatest at low frequencies and therefore, vibration limits in the range from 1 Hz to 80 Hz must be met. In accordance with CIBSE Guide D, in-car noise levels, machine room noise levels and lobby noise levels must be under control. The basic solution to these problems is to reduce the noise generated by a moving car. It is therefore a necessity to make a revolution on the external structure of elevator cars so as to keep the noise levels, vibration levels and drag force to a minimum subject to a limited size of hoistway. The initial step is to produce a comprehensive, realistic and reasonably accurate mechanical model of a super-high-speed elevator car inside a conventional hoistway so that the aerodynamic properties can be studied thoroughly. A 1-dimensional initial study was carried out [1].

2 A REVIEW ON THE 1-DIMENSIONAL MODEL

A one-dimensional model was initially used to study the air flow pattern inside the hoistway. Lots of assumptions were made so that this model is very much different from the real situation but this model can give us an insight into the changing patterns of air flow when the elevator car is accelerating. The assumptions made are shown below:

a) An up-travelling car is simulated;
b) The leakage of air downwards around the car is neglected;
c) The gravity of air is neglected and hence the potential energy of air;
d) The leakage of air through landing doors is neglected;
e) The irregular shape of car and hoistway is not taken into account of.

The typical aerodynamic characteristics, i.e. pressure distributions, is revealed when the speed and acceleration are high. A linear hoistway is assumed where x represents the linear space above an upward accelerating car. The simplified mathematical model adopted is the 1-dimensional inviscid flow model and the governed equations are as follows:

$$\frac{\partial \rho}{\partial t} + \frac{\partial (\rho V)}{\partial x} = 0 \qquad (1)$$

$$\frac{\partial (\rho V)}{\partial t} + \frac{\partial}{\partial x}(\rho V^2 + p) = 0 \qquad (2)$$

$$\frac{\partial}{\partial t}\left[\rho \left(e + \frac{1}{2}V^2 \right) \right] + \frac{\partial}{\partial x}\left\{ V \left[\rho \left(e + \frac{1}{2}V^2 \right) + p \right] \right\} = 0 \qquad (3)$$

Here, ρ is the density of air, being assumed as constant throughout the simulation; V is the instantaneous velocity of air at level x; p is the instantaneous pressure at level x; e is the specific internal energy of ideal gas defined below by equation (4). These three equations are the conservation forms of the continuity, x-momentum and energy equations respectively.

$$e \triangleq c_v T = \frac{p}{(\gamma - 1)\rho} \quad (4)$$

Here, γ is the specific heat ratio. With the aid of equation (4), it can be noticed that equations (1) to (3) contain three dependent variables, namely V, ρ and p.

3 INTRODUCTION TO THE MULTI-GRID METHOD

The flow in the hoistway with an accelerating or decelerating car is very complicated and unsteady due to the compressibility and strong turbulentibility of air. The calculation domains always change with the moving car. In this way, the calculation grid must be rebuilt with time during the whole simulation process. The air is strongly compressible, especially when the car moves near the bottom or the top of the hoistway, resulting in the production of some kinds of compress waves. The flow is highly turbulent so that the flow and the side of the lift car must be carefully handled.

There are many kinds of different schemes, numerical models and commercially available software packages for computational fluid dynamics (CFD) and all these can, in a certain way, assist us to solve our problem. MacCormack explicit algorithm [3,4] is one of the widely used methods for calculating flow with compressible turbulence and this algorithm has many advantages such as the convenience in vectoring, programming, understanding, wide compatibility and low memory requirement. Multi-grid [5,6] technique is a numerical scheme that has the ability to increase the convergence speed for the calculation. Some research results indicate that the convergence speed for the MacCormack explicit algorithm can increase 2.1 times by using the multi-grid technique.

The multi-grid method was first introduced in 1961 for solving Poisson equation by Fedorenko and then Backvalov discussed the variable-coefficient boundary value problem in 1969. Ni [7] introduced a multi-grid acceleration scheme with one-step Las-Wendroff algorithm and applied it to the solution of homoenthalpic Euler equations. Johnson extended this technique to the more general case of two-step MacCormack explicit algorithm to solve 2-D Euler equations by a finite-volume method.

The characteristic feature of multi-grid method is the combination of the fine-grid smoothing and the coarse-grid correcting steps. During the calculation in the fine grid, the defect, i.e. residuum, is not necessarily reduced but "smoothed". By following the correction step, the discrete solution is improved by means of an auxiliary equation in a coarser grid. The result is a very fast and effective iterative process. This paper deals with the development of an efficient explicit multi-grid algorithm for multi-dimensional unsteady compressible turbulence flow. This multi-grid algorithm is based on Ni's and Johnson's approaches on the macCormack fine-difference scheme and the estimation of the Jacobian matrices is not required. The flows in the hoistway with three kinds of external shape of an elevator car are studied. For convenience, the 3-D governing equations are prepared but the solution is based on a 2-D simulation so that the same set of equations can be used again in future for a full 3-D study.

4 GOVERNING EQUATIONS

The 3-D Reynolds-Averaged N-S equations, with Boussinesq eddy-viscosity formulation, are written in full form and transformed from the Cartesian co-ordinate system (x, y, z) into the Arbitrary co-ordinate system (ξ, η, ζ), as shown below:

$$\frac{\partial Q}{\partial t} + \frac{\partial}{\partial \xi^k}\left(C_e^k + C_\gamma^k\right) = 0 \quad k = 1, 2, 3$$

$$\text{where} \quad \begin{bmatrix} \xi^1 \\ \xi^2 \\ \xi^3 \end{bmatrix} = \begin{bmatrix} \xi \\ \eta \\ \zeta \end{bmatrix} \qquad Q = \begin{bmatrix} \rho \\ \rho\, u^j \\ \rho\, e \end{bmatrix}$$

$$C_e^k = \left(\frac{\partial \xi^k}{\partial t} + u^l \frac{\partial \xi^k}{\partial x^l}\right) Q + J^{-1} \begin{bmatrix} 0 \\ p\delta_j^k \dfrac{\partial \xi^k}{\partial x^j} \\ p u^l \dfrac{\partial \xi^k}{\partial x^l} \end{bmatrix} \tag{5}$$

$$C_\gamma^k = J^{-1} \begin{bmatrix} 0 \\ -\tau_{jl} \dfrac{\partial \xi^k}{\partial x^l} \\ -(u^l \tau_{lm} - q_m) \dfrac{\partial \xi^k}{\partial x^m} \end{bmatrix} \quad j = 1, 2, 3$$

and k, l, m = 1, 2, 3. J = det ($\partial \xi^k / \partial x^l$) is the Jacobian Matrix. The terms of the stress and heat flux are given in the non-dimensional forms as shown below:

$$\tau_{ij} = (\mu + \mu_t)\left[\left(\frac{\partial u^i}{\partial x^j} + \frac{\partial u^j}{\partial x^i}\right) - \frac{2}{3}\delta_{ij}\frac{\partial u^k}{\partial x^k}\right]$$

$$q_i = \left(\frac{\mu}{Pr} + \frac{\mu_t}{Pr_t}\right)\frac{1}{\gamma + 1}\frac{\partial h}{\partial x^i} \tag{6}$$

Here, μ is the viscosity and is given by Sutherland equation (non-dimensional form):

$$\mu = T^{\frac{3}{2}} \frac{1 + \dfrac{110.4}{T_\infty}}{T_\infty + \dfrac{110.4}{T_\infty}} \tag{7}$$

μ_t is the eddy viscosity and is given by Baldwin-Lomax turbulence model. The non-dimensional forms in the arbitrary coordinate system is shown below:

$$\mu_t = (\mu_t)_{inner} \quad y \le y_c \quad ; \quad \mu_t = (\mu_t)_{outer} \quad y > y_c \tag{8}$$

where y is the normal distance of the car from the wall and y_c can be decided by

$[\mu_t(y_c)]_{inner} = [\mu_t(y_c)]_{outer}$. In the inner regions of the boundary layer, the following equation applies:

$$(\mu_t)_{inner} = Re\ l^2\ \rho\ |\ \overline{\omega}\ | \tag{9}$$

where l is the mixing length as shown below:

$$\begin{aligned} l &= k\ y \left[1 - e^{\frac{y^+}{A^+}} \right] \\ y^+ &= y\ \frac{\sqrt{Re}\ \sqrt{\rho\ \tau_w}}{\mu_w} \qquad k,\ A^+ \ \textit{are constants} \end{aligned} \tag{10}$$

The corresponding formula for the outer region is shown below:

$$\begin{aligned} (\mu_t)_{outer} &= K\ C_{cp}\ F_{wake}\ F_{kleb}\ (y)\ \rho \\ \textit{where}\quad K\ ,\ C_{cp} &\ \ \textit{are constants} \\ F_{wake} &= \min \left\{ y_{\max}\ F_{\max}\ ,\ C_{wk}\ y_{\max}\ u_{Dif}^2\ F_{\max} \right\} \end{aligned} \tag{11}$$

y_{max} and F_{max} are determined by the maximum of the following equation:

$$F\ (y\ ) = y\ |\ \overline{\omega}\ | \left[1 - e^{-\frac{y^+}{A^+}} \right] \tag{12}$$

F_{kleb} is the Klebanoff intermittence factor given by the following equation:

$$F_{kleb} = \left[1 - 5.5 \left(\frac{C_{kleb}\ y}{y_{\max}} \right)^6 \right]^{-1} \qquad u_{Dif} = |\vec{u}|_{\max} - |\vec{u}|_{\min} \tag{13}$$

5 THE MULTI-GRID ALGORITHM

The author made use of the algorithm in other areas of application and those who are interested in them may refer to the two publications [8,9].

5.1 Fine-Grid Algorithm

On the fine grid, the explicit MacCormack algorithm is used in its unsplit form. MacCormack algorithm is a popular member within the class of Lax-Wendroff two-step schemes. It is given below in its forward-predictor-backward-corrector form;

$$\textit{Current solution is stored in array:} \quad \Delta\ Q_{i\ ,\ j\ ,\ k} \tag{14}$$

$$\text{Forward Predictor: } \overline{Q^{n+1}_{i,j,k}} = Q^{n}_{i,j,k} - \Delta t\, M$$
$$M = C^{1(n)}_{i+1,j,k} - C^{1(n)}_{i,j,k} + C^{2(n)}_{i,j+1,k} - C^{2(n)}_{i,j,k} + C^{3(n)}_{i,j,k+1} - C^{3(n)}_{i,j,k} \tag{15}$$

$$\text{Backward Corrector: } Q^{n+1}_{i,j,k} = \frac{1}{2}\left[Q^{n}_{i,j,k} + \overline{Q^{n+1}_{i,j,k}} \right] - \frac{\Delta t}{2} N$$
$$N = C^{1\overline{(n+1)}}_{i,j,k} - C^{1\overline{(n+1)}}_{i-1,j,k} + C^{2\overline{(n+1)}}_{i,j,k} - C^{2\overline{(n+1)}}_{i,j-1,k} + C^{3\overline{(n+1)}}_{i,j,k} - C^{3\overline{(n+1)}}_{i,j,k-1} \tag{16}$$
$$\text{where } C^{k} = C^{k}_{e} + C^{k}_{\gamma} \quad k = 1, 2, 3$$

Artificial dissipation is given by the following equation:

$$Q^{n+1} = Q^{n+1}_{i,j,k} + D_{i,j,k} \tag{17}$$

Residuals in the array are collected in the following way:

$$\Delta Q^{n+1}_{i,j,k} = Q^{n+1}_{i,j,k} - Q^{n}_{i,j,k} \tag{18}$$

Although the treatment shown above requires extra computational loading, a better accuracy and convergence can be obtained for the solution.

5.2 Artificial Dissipation

Terms of artificial dissipation consisting of second and forth differences are added to prevent odd-even point decoupling and to allow compress wave in the flow capturing respectively, especially for Euler solver. But for viscous flows, it is also necessary to use artificial dissipation for good convergence rate. There are many forms of artificial dissipative terms but they can be divided into two conceptually different models. The first model has been made popular by Jameson and Chima. The second model is the physically based dissipation developed by Dulibravich recently. In this paper, the dissipative model based on Jameson is used. The dissipative term, D, is given by:

$$D = \left(D_{\xi} + D_{\eta} + D_{\zeta} \right) Q \tag{19}$$

where D_{ξ} , D_{η} , D_{ζ} are dissipative operators in directions of ξ , η , ζ

In the ξ direction, the operator is given by:

$$D_{\xi} Q = \frac{J_{i,j,k}}{\Delta t}\left(\varepsilon^{(2)} Q_{\xi\xi} - \varepsilon^{(4)} Q_{\xi\xi\xi\xi} \right)$$
$$\text{where } \varepsilon^{(2)} = k^{(2)} \max\left(\gamma_{i+1} , \gamma_{i} , \gamma_{i-1} \right) \tag{20}$$
$$\varepsilon^{(4)} = k^{(4)} \max\left(0 , k^{(4)} - \varepsilon^{(2)} \right)$$

Here, $k^{(2)}$ and $k^{(4)}$ are user-specified coefficients and the values are $k^{(2)} = 1/4$ and $k^{(4)} = 1/256$ in this project. $\gamma_{i,j,k}$ represents an artificial dissipation sensor shown below:

$$\gamma_{i,j,k} = \frac{\left| \rho_{i+1,j,k} - 2\,\rho_{i,j,k} + \rho_{i-1,j,k} \right|}{\rho_{i+1,j,k} + 2\,\rho_{i,j,k} + \rho_{i-1,j,k}} \tag{21}$$

As a matter of fact, $\rho_{i,j,k}$ can be replaced by pressure $p_{i,j,k}$ as they are proportional to one another. In the smooth regions of flow, the dissipative terms are within the truncation error of the MacCormack algorithm and therefore they will not affect the accuracy of the fine-grid scheme. Second-order dissipation is usually added to prevent pro-compress wave oscillations. At places near to the existence of shock or compress wave, $\gamma_{i,j,k}$ is large and the second order difference dissipation becomes first order locally. The 2nd order dissipation coefficient is written in terms of density for computational efficiency.

5.3 Coarse-Grid Algorithm

Given the change in the fine-grid solution computed by one iteration of MacCormack algorithm, successively coarser grids are used to extend the change throughout the whole system. The coarse-grid propagation scheme used here is essentially the second half of one-step Lax-Wendroff scheme developed by Ni for two dimensional Euler equations. The first step of Ni's scheme computes changes at a grid point, and the second step distributes those changes to surrounding points. Johnson showed that the first step of Ni's scheme might be replaced by a variety of Lax-Wendroff schemes, including MacCormack's scheme. Furthermore, Johnson demonstrated that dissipative effects had a local character in viscous flows. Therefore, the so-called "Convective Coarse-Grid Acceleration Scheme" used here is solely on the Euler equations. The coarse-grid scheme is entirely independent of the viscous terms retained, the turbulence model used, or any artificial dissipation added to the fine grid. But Johnson's coarse-grid scheme need the calculation of Jacobian matrix which is time and memory consuming for 3-D simulation. In order to overcome such shortcomings, a coarse grid scheme based on Taylor series is used. Given a fine-grid solution, $Q_{i,j,k}$ and a fine grid change as shown in equation (18), the coarse-grid change can be estimated by using a Talor series:

$$\begin{aligned} \Delta Q_{i,j,k}^{n+2} &= \Delta Q_{i,j,k}^{n+1} + \Delta t\,(\Delta Q_{i,j,k}^{n+1})_t + 0\,(\Delta t)^2 \\ &= \Delta Q_{i,j,k}^{n+1} - \Delta t\,\frac{\partial(\,\Delta C^l\,)^{n+1}}{\partial \xi^l} \end{aligned} \tag{22}$$

By using the Johnson's "Convective Coarse-Grid Acceleration Scheme", equation (22) can be implemented on a coarse grid as shown below:

$$\begin{aligned} (\,\Delta Q\,)_{i,j,k}^{(n+2)}\,|_{2h} = \frac{1}{8}\Big\{ & [\Delta Q - \Delta t(\Delta C^l)]_{i+1,j+1,k+1}^{(n+1)} + [\Delta Q - \Delta t(\Delta C^l)]_{i+1,j+1,k-1}^{(n+1)} \\ & + [\Delta Q - \Delta t(\Delta C^l)]_{i+1,j-1,k+1}^{(n+1)} + [\Delta Q - \Delta t(\Delta C^l)]_{i+1,j-1,k-1}^{(n+1)} \\ & + [\Delta Q - \Delta t(\Delta C^l)]_{i-1,j+1,k+1}^{(n+1)} + [\Delta Q - \Delta t(\Delta C^l)]_{i-1,j+1,k-1}^{(n+1)} \\ & + [\Delta Q - \Delta t(\Delta C^l)]_{i-1,j-1,k+1}^{(n+1)} + [\Delta Q - \Delta t(\Delta C^l)]_{i-1,j-1,k-1}^{(n+1)} \Big\} \end{aligned} \tag{23}$$

The fine-grid MacCormack scheme is used to advance the solution by one time step, giving Q^{n+1} and ΔQ^{N+1} for each grid point. By choosing a suitable value of h for a coarse grid, equation (23) can be used to determine ΔQ^{n+2} at the coarse-grid points. On the boundaries, ΔQ^{n-1} is taken to be zero. Values of ΔQ^{n+2} at intermediate fine-grid points are estimated by bilinear interpolation and the fine grid is updated using:

$$\Delta Q^{n+2} = Q^{n+1} + \Delta Q^{n+2} \qquad (24)$$

The process can be repeated by advancing from the fine grid to the coarse grid with each iteration. Since the right hand side of equation (23) only depends on fine-grid changes, the coarse grid scheme cannot affect the convergence of the solution. Hence, this multi-grid scheme retains fine-grid accuracy. Similarly, all physical viscous dissipation terms may be neglected on the coarse-grid without affecting a viscous solution on the fine grid. The number of points of a fine grid is expressible as $(n-1)2^{(p-1)}+1$ for integers p and n while p is the number of grid crossings and n is the number of intervals on the coarse grid.

6 THE COMPUTER SIMULATION

The 2-D flows are calculated by a 3-level V-cycle, or sawtooth cycle, multi-grid sequencing as shown in Fig. 1. The region under calculation, which is a cylindrical car accelerating inside a cylindrical hoistway, is shown in Fig. 2. Three kinds of car shape are simulated. The maximum speed of the car is 25 m/s. The first one is a flat top design, which is the conventional design, shown in Fig. 3. The second one is a conical top design, shown in Fig. 4 while the third one is a spherical top design, shown in Fig. 5.

From Fig. 3, 4 and 5, we are able to see the velocity field around the elevator car. Both the flat top and conical top design have sudden change in the velocity fields at the top and bottom corners of the elevator car. However, there is no sudden change in velocity field at the upper corner of the car with spherical top design. The authors believer that a sudden change in the velocity field is the major source of excessive noise and vibration. Fig. 6 shows the distribution of air pressure on the car side, at time t = 11 s after the commencement of movement. It can be seen that the spherical top design has got the lowest pressure distribution, perhaps due to the stream-line external appearance. Fig. 7 shows the pressure distribution along the center-line of the hoistway from the car top towards the roof at time t = 11 s. It can also be seen that the spherical top design gives the best pressure distribution inside the hoistway. We shall then have reasons to believe that the spherical top design will experience the least noise and vibration problems as compared with the conventional design of flat top. All calculations are provided with an initial speed of zero and all cars start to accelerate from the bottom floor.

7 CONCLUSIONS

The background of the research project has been highlighted has been highlighted. As buildings are getting higher and higher, elevators of higher speed will become mandatory. However, super-high-speed elevators face problems such as excessive

vibration and noise. Therefore, special design of the car structure is necessary. The 1-D flow analysis was carried out and published. In this paper, a 2-D model has been developed, including the display of pressure distribution under three kinds of elevator car and also the simulation of leakage of air flow around the elevator car. The multi-grid algorithm, with fine and coarse alternation, has been employed to arrive at the solution and the governing equations are included in this paper. Three kinds of shape for the exterior of an elevator car have been simulated and it has been found that the parabolic top design gives the best performance, which is in line with our common sense. From Fig. 5, we can still find an abrupt change in velocity field towards the bottom corner of the car. That implies not just the top of the car needs specific design but also the bottom as well.

Irregular shapes of both the hoistway and the elevator car will be taken into account of in the future so that a true 3-dimensional modelling can be carried out. It is hoped that some sort of irregular shapes for the car design will give even more superior performance, which may go against our common sense. In that case, only a comprehensive computational fluid dynamical simulation can really suggest the optimal car shape design for our future to provide elevator services for ultra-high-rise buildings of, say 150 storeys or more. Experimental approach using PIV will be the final step to verify the design results generated from this CFD approach.

8 ACKNOWLEDGEMENT

The project is financially supported by the Strategic Research Grant # 7000505 of the City University of Hong Kong. Most of the simulation works were carried out in the Intelligent Building Research Laboratory of City University of Hong Kong and the Beijing University of Aeronautics and Astronautics. The authors are also indebted to the support from the International Association of Elevator Engineers (Hong Kong - China Branch) which will become IAEE (China Branch) within a few months time.

9 REFERENCES

[1] Fortune J.W. (1995) Mega high-rise elevators, *Elevator World*, Vol. XLIII, No. 7, pp. 64-69.

[2] So A.T.P., Chow T.T., Shen G.X. and Yang H.W. (1996) An aerodynamic mathematical model for super-high-speed elevators, in Barney G.C. eds. *Elevator Technology 7, Proceedings of Elevcon '96*, IAEE, Barcelona, pp. 204-213.

[3] MacCormarck R.W. (1969) The effect of viscosity in hypervelocity impact cratering, *AIAA Paper*, 69-354.

[4] MacCormack R.W. (1981) A numerical method for solving the equation of compressible viscous flows, *AIAA Paper*, 81-0110.

[5] Chima R.V. et al (1983) Efficient solution of the euler and n-s equation with a vectorized multi-grid algorithm, *AIAA Paper*, 83-1893.

[6] Chima R.V. et al (1988) Comparison of three explicit multigrid method for euler and n-s equations, *NASA TM-88878*.

[7] Ni R.H. (1981) A multigrid scheme for solving euler equations, *AIAA Paper*, 81-1025.

[8] Yang H.W. (1994) An explicit multi-grid technique for 3-D viscous flow simulation, *ACTA Aeronautica Et Astronautica Sinica*, Vol. 15, No. 11.

[9] Yang H.W. (1996) An adaptive grid algorithm for computing high speed 3-D complex flows, *ACTA Aeronautica Et Astronautica Sinica*, Vol. 17 (to be published).

Time Step	1 2 ... ... n
Fine Grids	h h ... ... h
Coarse Grids	2h 2h ... ... 2h 4h 4h ... ... 4h ... ... mh mh ... ... mh

Fig. 1 The Multi-Grid Configuration

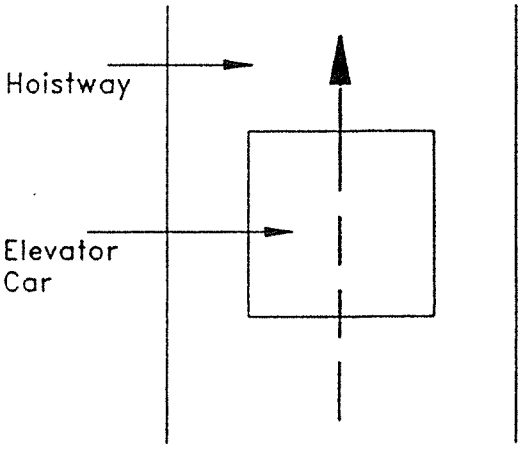

Fig. 2 Region under Simulation

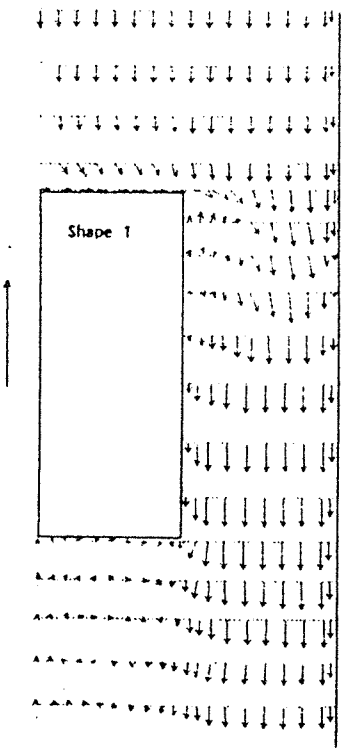

Fig. 3

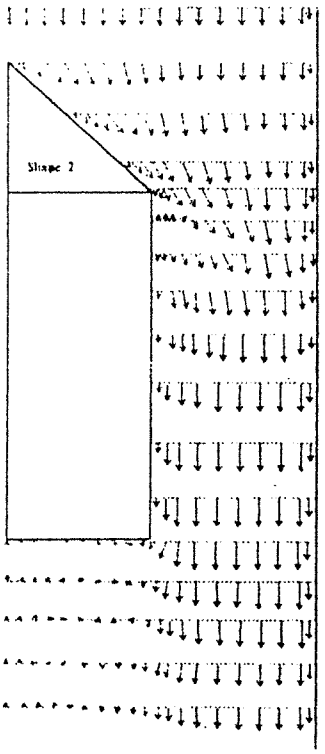

Fig. 4

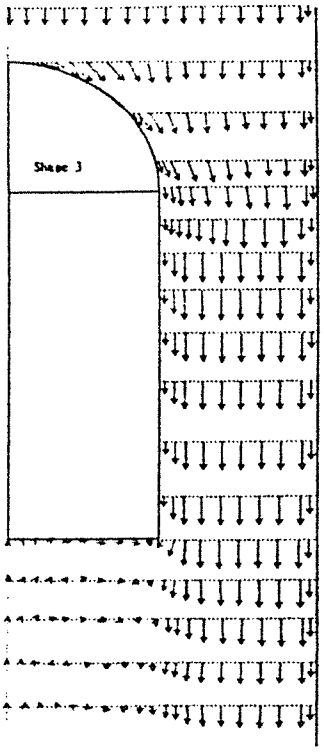

Fig. 5

Zooming View of Flow Fields around Three Kinds of Car Top Design

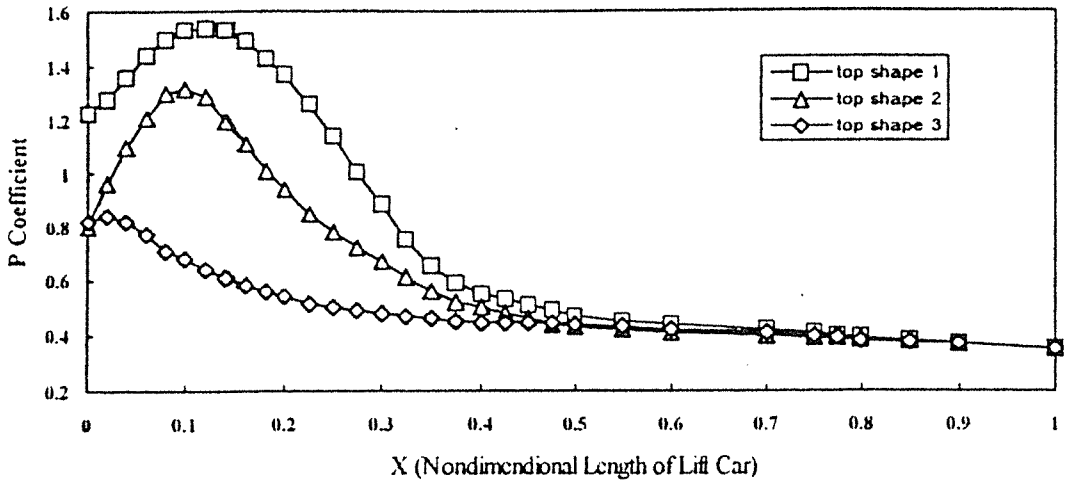

Fig. 6 Pressure Distributions along Elevator Car Wall

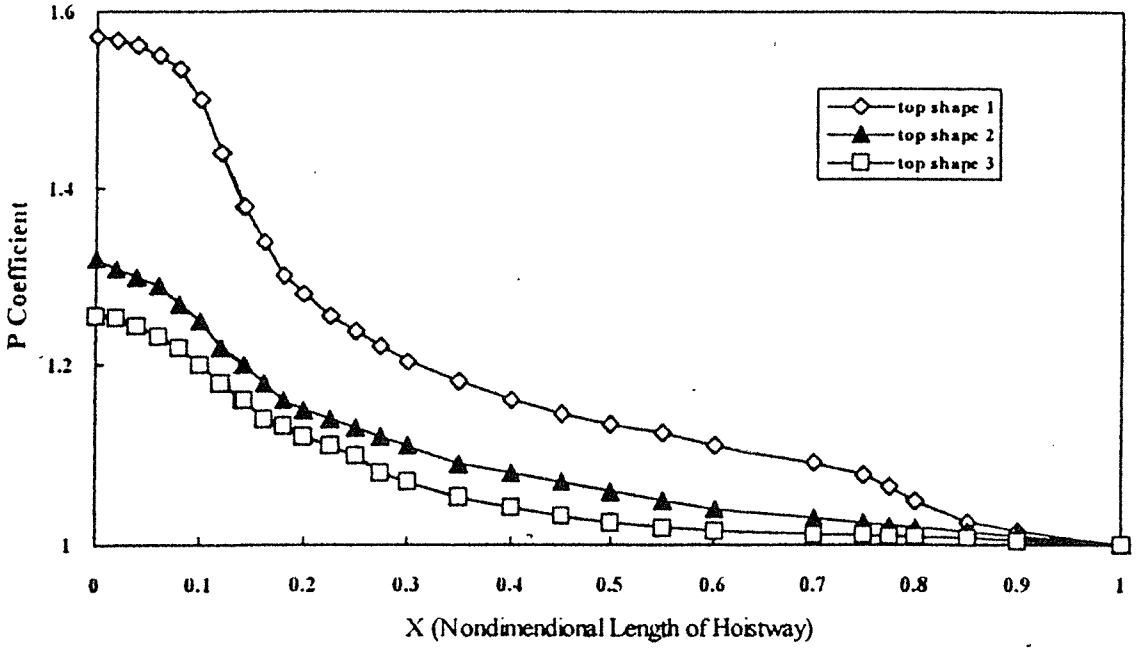

Fig. 7 Pressure Distributions along Centre Line of Hoistway about Car Top